Journal of Catalysis 299 (2013) 261–271

Contents lists available at SciVerse ScienceDirect

Journal of Catalysis

journal homepage: www.elsevier.com/locate/jcat

Influence of oxygen and pH on the selective oxidation of ethanol on Pd catalysts

David D. Hibbitts [a], Matthew Neurock [a,b,*]

[a] Department of Chemical Engineering, University of Virginia, Charlottesville, VA, United States
[b] Department of Chemistry, University of Virginia, Charlottesville, VA, United States

ARTICLE INFO

Article history:
Received 14 September 2012
Revised 13 November 2012
Accepted 14 November 2012
Available online 28 January 2013

Keywords:
Alcohol oxidation
Ethanol oxidation
Pd
DFT
Aqueous phase
Solvent effects

ABSTRACT

The selective oxidation of ethanol on supported Pd is catalytically promoted by the presence of hydroxide species on the Pd surface as well as in solution. These hydroxide intermediates act as Brønsted bases which readily abstract protons from the hydroxyl groups of adsorbed or solution-phase alcohols. The C_1—H bond of the resulting alkoxide is subsequently activated on the metal surface via hydride elimination to form acetaldehyde. Surface and solution-phase hydroxide intermediates can also readily react with the acetaldehyde via nucleophilic addition to form a germinal diol intermediate, which subsequently undergoes a second C_1—H bond activation on Pd to form acetic acid. The role of O_2 is to remove the electrons produced in the oxidation reaction via the oxygen reduction reaction over Pd. The reduction reaction also regenerates the hydroxide intermediates and removes adsorbed hydrogen that is produced during the oxidation.

1. Introduction

The selective oxidation of alcohols in aqueous media provides an attractive route to organic acids from biorenewable feedstocks. For example, glycerol, produced from the transesterification of fatty acids [1,2], can be oxidized to form glyceric and tartronic acids used in pharmaceutical and cosmetics industries [3]. Similarly, hydroxymethylfurfural (HMF) produced from the dehydration of fructose [4] can be oxidized to produce 2,5-furandicarboxylic acid (FDCA), which can be used to create PET plastics, offsetting the demand for oil-based terephthalic acid [5].

Aerobic oxidation of alcohols is often carried out over supported noble metal catalysts, including Pt, Pd, and Au [6,7]. Liquid-phase in situ XANES experiments have confirmed that these catalysts are active in their reduced, metallic state during oxidation [8,9]. Kinetic studies reported in the literature suggest that the mechanism proceeds via the formation of an aldehyde intermediate and that activity and selectivity to the acid product increases significantly when the reactions are carried out at high pH [6]. While Pt and Pd demonstrate some activity at neutral and slightly acidic pH, the reaction is inactive over Au at neutral pH for the activation of various alcohols [10–14].

Rigorous isotopic labeling studies along with density functional theory (DFT) calculations were recently carried out by Zope et al. [12] to determine the roles of both molecular oxygen and hydroxide in the mechanisms of glycerol and ethanol oxidation over supported Au catalysts. The results from this work suggest that the metal-solvent interface provides a unique environment that promotes the oxidation of the alcohol via the hydroxide present on the surface as well as in solution. Molecular oxygen, which is necessary to carry out this reaction, is an indirect reagent that removes electrons from the catalytic metal surface produced during oxidation. This occurs via the reduction with water as summarized in Eq. (1b). The oxidation mechanism on supported Au is very similar to the mechanism of electrooxidation on supported Au electrodes (with the exception of the applied potential). In the direct alcohol fuel cells, the rate of oxidation that occurs at the anode is balanced by the rate of oxygen reduction at the cathode [15–18].

$$CH_3CH_2OH + 4OH^- \rightarrow CH_3COOH + 3H_2O + 4e^- \quad (1a)$$

$$O_2 + 2H_2O + 4e^- \rightarrow H_2O_2 \rightarrow 4OH^- \quad (1b)$$

However, other investigators have suggested that molecular oxygen first dissociates to form atomic oxygen on the surface, which subsequently behaves as a Brønsted base on the surface to carry out the oxidation chemistry, similar to the role of hydroxide above [19]. Oxygen is known to dissociate over Pt and Pd surfaces [20,21], and although oxygen dissociation is not observed over Au(111) [22], there is the possibility that low-coordinated sites or defect sites on Au nanoparticles may dissociate oxygen, and the presence of oxygen atoms can increase the rate of oxygen dissociation due to the formation of partially oxidized Au clusters [22]. Furthermore, over Pt and Pd catalysts, there is some activity reported at neutral or slightly acidic pH [23,24], suggesting that there are pathways

* Corresponding author at: Department of Chemical Engineering, University of Virginia, Charlottesville, VA, United States.
E-mail address: mn4n@virginia.edu (M. Neurock).

0021-9517/$ - see front matter © 2012 Elsevier Inc. All rights reserved.
http://dx.doi.org/10.1016/j.jcat.2012.11.016

available which do not require large amounts of hydroxide to be present. The mechanisms, as discussed in the next section, vary significantly across the literature, and a thorough examination of the reaction network has not yet been presented.

To evaluate these possible mechanisms, density functional theory (DFT) calculations were performed to establish the activation barriers and reaction energies for a large set of elementary reactions. The work examined herein will focus on the selective oxidation of ethanol, which follows similar kinetics and mechanisms as glycerol and other polyols but is more computationally tractable. We examine Pd, as it is known to readily dissociate oxygen and reduce O^* and OH^* intermediates that result to form water [20,25]. Pd, however, has a much lower tendency to completely oxidize the alcohol to CO_2 and H_2O as a result of the difficulty in activating C—C bonds on Pd compared to on Pt [6].

2. Proposed mechanisms

2.1. Ethanol dehydrogenation

The dehydrogenation of ethanol (CH_3CH_2OH) to acetaldehyde (CH_3CHO) can proceed by the initial activation of either the C—H or O—H bond of ethanol as shown in Eqs. (2a)–(2c). Studies of ethanol oxidation over Pt and Pd electrocatalysts suggest that C—H activation occurs via the oxidative insertion of the metal into the C—H bond to form hydroxyethylidene (CH_3CH^*OH) and hydride (H^*) surface intermediates [16,17,26] as shown in Eq. (2a). Alternatively, studies in the heterogeneous catalysis literature report that alcohol oxidation proceeds via the initial activation of the O—H bond to form ethoxide ($CH_3CH_2O^*$) and H^* surface intermediates [6,7,23] as shown in Eq. (2b). In solution, an equilibrium exists between the ethanol and the ethoxide ion through base-catalyzed deprotonation as shown in Eq. (2c).

$$CH_3CH_2OH^* \rightarrow CH_3CHOH^* + H^* \rightarrow CH_3CH{=}O^* + 2H^* \quad (2a)$$

$$CH_3CH_2OH^* \rightarrow CH_3CH_2O^* + H^* \rightarrow CH_3CH{=}O^* + 2H^* \quad (2b)$$

$$\begin{aligned} CH_3CH_2OH + OH^- &\leftrightarrow CH_3CH_2O^- + H_2O \\ &\leftrightarrow CH_3CH_2O^* + e^- + H_2O \end{aligned} \quad (2c)$$

Adsorbed oxygen or hydroxide can also act as a Brønsted base to partially reduce the hydrocarbon as shown below in Eq. (3). This mechanism is supported by kinetic studies which suggest a Langmuir–Hinshelwood mechanism [27,28] where the rate-limiting step involves the reaction between surface oxygen and an ethanol intermediate [19]. We recently demonstrated that hydroxide behaves as a Brønsted base on Au and Pt(1 1 1) surfaces where it abstracts the more acidic proton of the alcohol [12].

$$\begin{aligned} CH_3CH_2OH^* + 2O^* &\rightarrow CH_3CH_2O^* + OH^* + O^* \\ &\rightarrow CH_3CH{=}O^* + 2OH^* \end{aligned} \quad (3a)$$

$$\begin{aligned} CH_3CH_2OH^* + 2OH^* &\rightarrow CH_3CH_2O^* + H_2O^* + OH^* \\ &\rightarrow CH_3CH{=}O^* + 2H_2O^* \end{aligned} \quad (3b)$$

Previous theoretical results suggest that the high alkalinity in this reaction would result in a high coverage of hydroxide groups on the metal surface which would facilitate the C—H activation of ethanol to form the adsorbed hydroxyethylidene intermediate as is shown in Eq. (4) [17]. This work however was carried out using small Pd clusters (14–20 atoms) and does not consider the ethoxide route or the possibility of aqueous-phase deprotonation. It also does not consider the possible effects of hydroxide groups upon the subsequent oxidation of acetaldehyde to acetic acid (CH_3COOH).

$$\begin{aligned} CH_3CH_2OH^* + OH^* + {}^* &\rightarrow CH_3CHOH^* + H_2O^* + {}^* \\ &\rightarrow CH_3CH{=}O^* + H^* + H_2O^* \end{aligned} \quad (4)$$

2.2. Acetaldehyde oxidation

The oxidation of the aldehyde to the acid can proceed via two competing intermediates (Eqs. (5a)–(5c)): acetyl (CH_3CO), which is the more commonly proposed route in the literature [6,16,18,23] and ethoxy-diol ($CH_3CH(OH)O$), which can be formed on the surface as well as in solution [7,12,23]. These steps are presented in Eq. (5). Other routes involving the oxidation of the aldehyde, however, may also exist.

$$\begin{aligned} CH_3CHO^* + OH^* + {}^* &\rightarrow CH_3CO^* + H^* + OH^* \\ &\rightarrow CH_3COOH^* + 2^* \end{aligned} \quad (5a)$$

$$CH_3CHO^* + OH^* \rightarrow CH_3CH(OH)O^* + {}^* \rightarrow CH_3COOH^* + H^* \quad (5b)$$

$$\begin{aligned} CH_3CHO + OH^- + 2^* &\rightarrow CH_3CH(OH)O^- + 2^* \\ &\rightarrow CH_3CH(OH)O^* + e^- \\ &\rightarrow CH_3COOH^* + H^* \end{aligned} \quad (5c)$$

These pathways alone, for example, do not explain isotopic labeling studies performed by multiple investigators, which show that the oxidation of ethanol [12,29], glycerol [12], and other alcohols [5] with $H_2{}^{18}O$ labeled water in alkaline media result in the formation of the acetate product which contains multiple ^{18}O groups. This suggests that at some point within the mechanism, an intermediate with an equivalence between the ^{16}O on the alcohol intermediate and the ^{18}O in solution is formed. One possibility for this equivalence is the aqueous-phase hydration of the aldehyde to form a geminal diol as shown in Eq. (6). If this process is equilibrated, the aldehyde can exchange its oxygen with that of the labeled oxygen in water, which can lead to two ^{18}O being observed in the acid product.

$$\begin{aligned} RCHO + OH^- + H_2O &\leftrightarrow RCH(OH)O^- + H_2O \\ &\leftrightarrow RCH(OH)_2 + OH^- \end{aligned} \quad (6)$$

The gem-diol intermediate, once formed, can subsequently dehydrogenate to form the corresponding acid product, which subsequently deprotonates in basic media to form the corresponding carbonate.

2.3. Role of oxygen

During aerobic alcohol oxidation, oxygen is reduced to form water, thus removing electrons from the catalyst surface. This reduction can occur in various ways: Oxygen can dissociate to form atomic oxygen on the surface, which can react with adsorbed atomic hydrogen formed from oxidation reactions as shown in Eq. (7a) [30–32]. In this case, oxygen is merely a hydrogen acceptor, removing electrons from the metal and adsorbed hydrogen from the surface, if that is oxygen's only purpose, then another hydrogen acceptor, such as an olefin, can be substituted for O_2 in order to remove the electrons and adsorbed hydrogen as presented in Eq. (7b). Hayashi et al. [33] have shown that for the selective oxidation of alcohols to aldehydes, the reaction is active in the absence of oxygen under an ethylene atmosphere, demonstrating that the oxidative dehydrogenation of alcohols does not require O_2 present, and it merely requires an electron and H^* acceptor (such as ethylene). They did not report any further oxidation to acid products. Alternatively, atomic oxygen can act as a Brønsted base as previously discussed, directly abstracting hydrogen from the alcohol as shown in Eq. (3a). A third possibility is that O_2

dissociates on the surface to form atomic oxygen which readily oxidizes strongly-bound CO intermediates to CO_2 [34].

$$O_2 + 4H^* \rightarrow 2O^* + 4H^* \rightarrow 2OH^* + 2H^* \rightarrow 2H_2O^* \quad (7a)$$

$$CH_3CH_2OH^* + CH_2{=}CH_2^* \rightarrow CH_3CH{=}O^* + CH_3CH_3^* \quad (7b)$$

$$1/2O_2 + CO^* \rightarrow CO_2 + ^* \quad (7c)$$

In this work, we carry out first-principle density functional theory calculations to examine the role of adsorbed oxygen and hydroxide intermediates for various possible pathways of ethanol oxidation over a model Pd(1 1 1) surface. Pd was chosen due to its ability to dissociate O_2, creating active O^* species on the surface (unlike Au), while maintaining high selectivity (unlike Pt which frequently over-oxidizes the alcohol to CO_2). All of the calculations reported herein, unless otherwise noted, were carried out on Pd(1 1 1) in an aqueous media in order to capture the effect of the solvent phase. The computed activation barriers and reaction energies indicate that the dehydrogenation of ethanol to acetaldehyde occurs via ethoxide under high pH conditions. Hydroxide groups on the surface or in solution facilitate O—H activation through the direct interaction of hydroxide with the alcohol as previously suggested [12]. Oxygen appears to be required to remove electrons from the catalyst surface and regenerate the active hydroxide intermediate. However, the activation barriers for certain C—H or O—H activation steps are reduced if atomic oxygen is present to act as a Brønsted base, similar to Eq. (3a) above. This can explain the observed activity over Pt and Pd catalysts in absence of base, although, across all reactions, OH^*-assisted C—H or O—H activation has lower barriers than O^*-assisted C—H or O—H activation.

3. Computational methods

First-principle DFT calculations were carried out using the Vienna *ab initio* simulation package (VASP) [35–37]. The planewaves were constructed with an energy cutoff of 396 eV and Vanderbilt ultrasoft pseudopotentials [38,39] with real space projection operators defining the features of the core region. The correlation and exchange energies were determined using the Perdew–Wang 91 (PW91) form of the generalized gradient approximation (GGA) [40]. The binding energy of each adsorbate was calculated as:

$$E_{BE} = E_{surf+ads} - E_{surf} - E_{ads}$$

where $E_{surf+ads}$, E_{surf}, and E_{ads} are the energies of the surface-adsorbate complex, the surface, and the adsorbate in vacuum, respectively. It is important to note that this formal definition of binding energy is not as kinetically-relevant as a definition in which the reference state takes into account solvation of the adsorbate and solvent exchange on the surface. For this reason, the binding energies will be over-predicted, and phenomena such as desorption should be more facile in real systems. Furthermore, the free energy of adsorption would have to take into account the entropic effects of reorganizing the solution as well as the changes in entropy of the adsorbate between the aqueous and the adsorbed phases.

The binding energy calculations are referenced to a bare metal surface and the adsorbate isolated in the gas phase. The optimized structures and energies for all of isolated gas-phase molecules (E_{ads}) were calculated spin-polarized with the species in an $18 \times 18 \times 18$ Å unit cell using the γ-point version of VASP. The structures were optimized until the max atom force was less than 0.05 eV/Å; the forces were obtained using a fast Fourier transform (FFT) grid with a cutoff of twice the planewave cutoff; the wavefunctions were converged to within 10^{-6} eV.

All calculations upon metal surfaces were carried out non-spin-polarized. A 3×3 unit cell lattice was chosen in order to accommodate the reacting species with minimal interaction between supercells. The Pd(1 1 1) surface was modeled with four metal layers and a vacuum size of 18 Å separating the periodic structure in the *z*-direction. The top two layers of the metal were allowed to relax, while the lower two layers were fixed in their bulk lattice positions. When present, the aqueous solvent was modeled using multilayers of a hexagonal bilayer structure similar to previously published work [12,41–43]. On the 3×3 metal lattice, there are six water molecules per solvent bilayer, and four bilayers were included in the *z*-direction. In these bilayers, the water molecules have four hydrogen bonds with their neighbors, similar to the hexagonal close packed structure of ice. At the metal/water interface, three of the six water molecules weakly adsorb in atop positions while the other three hydrogen bond with the nearest bilayer of solvent. In order to accommodate reacting intermediates, one or more of the weakly adsorbed water molecules were removed to create vacancies at the surface. For all optimizations and transition state searches, the water was allowed to fully relax in all directions. While this model allows us to assess the effects of local solvent molecules and captures some of the longer-range effects, such as the solvent-induced dipole effect, it does not accurately capture liquid water solvent, which would require the simulation of dynamics along the reaction trajectories for up to 10^6 different configurations to provide statistical relevance which is not possible at the quantum mechanical level for metal/solvent interfaces.

The structures were optimized using a two-step approach at a k-point mesh of $3 \times 3 \times 1$, and the energy is subsequently computed in a third and final step at a $6 \times 6 \times 1$ k-point mesh as shown in Table 1. To test this three-step system, a sample of intermediates were optimized using a $6 \times 6 \times 1$ k-point mesh and an FFT grid size $2\times$ the planewave cutoff to a force below 0.05 eV/Å. The results reveal a difference of binding energies <0.02 eV. To test the force convergence criteria of 0.05 eV/Å, a selection of intermediates was converged to forces less than 0.01 eV/Å in the second step. The differences in these two methods resulted in changes in binding energy <0.02 eV.

For reactions, the activation barriers were obtained as:

$$A + B \rightarrow TS \rightarrow C + D$$

$$E_{ACT} = E_{TS} + \delta E_{surf} - E_{surf+A} - E_{surf+B}$$

$$E_{RXN} = E_{surf+C} + E_{surf+D} - E_{surf+A} - E_{surf+B}$$

where $E_{surf+ads}$, E_{surf}, and E_{TS} are the energies of the adsorbed intermediate (A, B, C, or D), the surface and the transition state, respectively, and δ refers the surface stoichiometric factor. This factor arises due to the choice of a reference state in which the reacting species are "infinitely" separated on the catalyst surface, so that any attractive or repulsive interactions between the reacting species are accounted for by the activation barrier.

The structures of the transition states were determined using nudged elastic band (NEB) [44] along with dimer [45] methods. The NEB method was used to optimize a series of intermediate structures (images) taken at equal distances along the reaction path in order to minimize the forces on each structure normal to reaction path and establish an estimate of the transition state structure. The transition state structures were further refined by the dimer method [45], which uses two images with a very small

Table 1
Three-step scheme for surface DFT calculations.

	Step 1	Step 2	Step 3
Wavefunction convergence	10^{-4}	10^{-6}	10^{-3}
FFT grid size	1.5×	2.0×	1.5×
k-Point mesh	$3 \times 3 \times 1$	$3 \times 3 \times 1$	$6 \times 6 \times 1$

distance between them (a "dimer") together with an algorithm which allows the dimer to move up along the potential energy surface to a saddle point with a single negative eigenmode.

NEB calculations were carried out using 16 images using a $3 \times 3 \times 1$ k-point mesh and an FFT grid size $1.5\times$ the planewave cutoff; the wavefunctions were converged to within 10^{-4} eV. The maximum force on each atom was converged to 0.20–0.50 eV/Å depending on the quality of the initial path and ability of the algorithms. As stated, the NEB calculations were used only to provide an initial guess to the dimer algorithm, so forces lower than 0.50 eV/Å are not necessary. The dimer algorithm was then performed using a $3 \times 3 \times 1$ k-point mesh and an FFT grid size $2\times$ the planewave cutoff; the wavefunctions were converged to within 10^{-6} eV. The distance between the dimers was set to 0.01 Å, and the dimer was allowed to rotate four times or until the rotational force fell beneath 1 eV/Å. The max atom force was converged to less than 0.05 eV/Å. As with the binding energy calculations, the energy of the transition state was then determined using a $6 \times 6 \times 1$ k-point mesh with the same parameters specified in Step 3 of Table 1.

4. Results and discussion

The results for the all of the elementary reaction steps studied on the Pd(1 1 1) surface in the presence of aqueous media are summarized in Fig. 1. All of the C—H and O—H activation steps reported were examined on the bare Pd surface, on Pd surfaces with surface oxygen (O^*) or surface hydroxide (OH^*) intermediates to act as Brønsted bases. In general, many of the OH^*-assisted C—H and O—H activation steps have lower barriers than O^*-assisted or direct metal atom insertion reactions. All of the barriers for steps involving C—H activation by O^* have barriers that are over 100 kJ/mol and are significantly higher than those on the metal or via OH^*.

4.1. Ethanol dehydrogenation

Ethanol can deprotonate in solution, forming an ethoxide anion, in an equilibrium-controlled reaction followed by adsorption of the ethoxide anion onto the catalyst surface. Ethanol can also adsorb on the Pd surface and subsequently react with chemisorbed $^*OH$ to form an adsorbed ethoxide intermediate. The barrier for this reaction (Rxn 1c) which is 29 kJ/mol is largely due to the energy required to restructure the local solvent shell, as shown in Fig. 2 and Table 2 (which shows that the barrier increases with the inclusion of solvent in the calculation). Since ethanol, the ethoxide anion, and hydroxide are also in equilibrium with their adsorbed species (Eq. (8)), increasing the pH of the system leads to an increase in coverage of the ethoxide intermediate. The bound ethoxide intermediate can subsequently undergo hydride elimination to form acetaldehyde with a barrier of 51 kJ/mol (Rxn 3a).

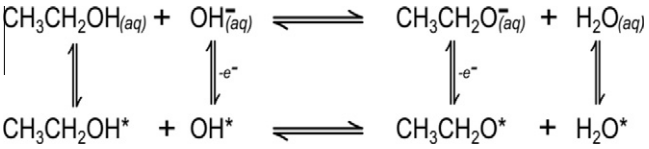

(8)

However, for systems at neutral or slightly acidic conditions, hydroxide may not be present at high enough concentrations to carry out the O—H activation of ethanol. If O^* is present at high coverages (due to O_2 or OOH dissociation), it can also carry out O—H activation of ethanol via proton abstraction with a barrier of 80 kJ/mol (Rxn 1b). However, if the O^* coverage is low, it is more likely that the exposed metal surface sites carry out the initial activation of ethanol via an oxidative insertion of the metal into the alpha C_1—H bond, as shown in Rxn 2a, to form hydroxyethylidene which has an activation barrier of 84 kJ/mol. (Compared to the barrier of 131 kJ/mol to activate the O—H bond of ethanol on Pd to form the ethoxide intermediate, Rxn 1a.)

As shown by the reaction network sketched in Fig. 1, if the initial activation occurs at the C_1 carbon, forming hydroxyethylidene (Rxn 2), multiple routes exist toward the acid product which do not produce the observed aldehyde intermediate. Although these alternative intermediates are not observed, it is important to establish whether the aldehyde is a primary intermediate or just an observed by-product. We therefore examined the various paths that can occur which include the following: oxidation via OH^*-addition to the carbon to form a geminal diol intermediate ($CH_3CH(OH)_2$,

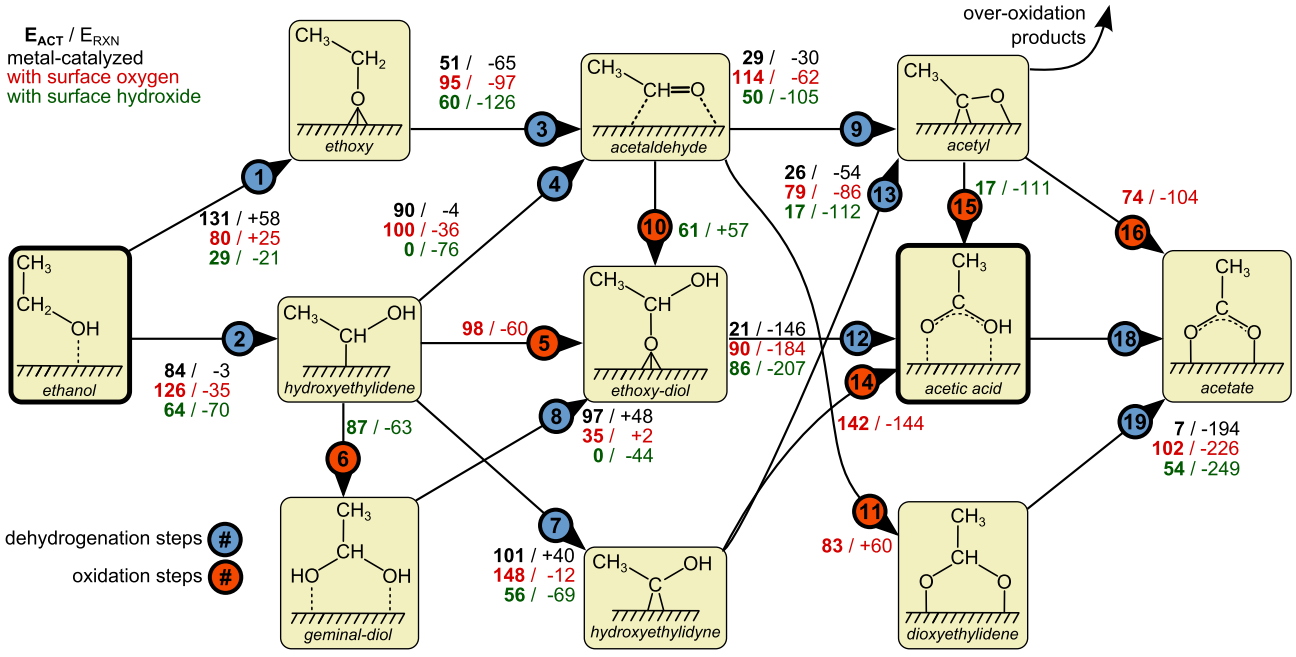

Fig. 1. Reaction network for the oxidation of ethanol to acetic acid or acetate products. DFT-calculated activation barriers over Pd(1 1 1) with solvent present are shown in bold. Reaction 18, the conversion of acetic acid to acetate, was not modeled.

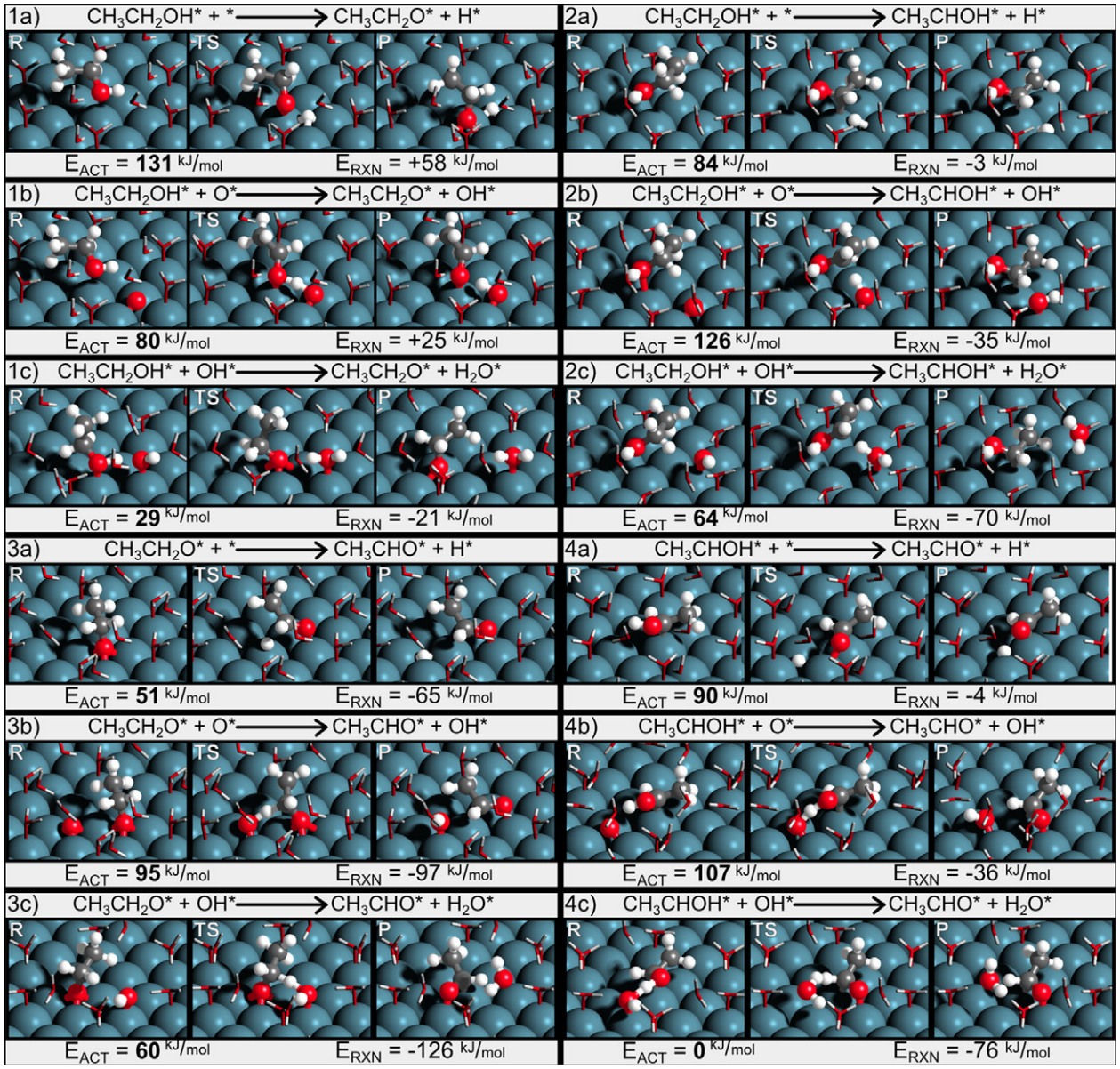

Fig. 2. Elementary O—H and C—H activation steps involved in the dehydrogenation of ethanol to acetaldehyde. The DFT-calculated reactant, transition and product states along with their activation barriers (E_{ACT}) and energies of reaction (E_{RXN}) are shown for both the hydroxyethylidene and ethoxide routes. Each dehydrogenation step was modeled over a bare surface, with O* and with OH* acting to abstract the hydrogen. Only the lowest layer of solvent (out of the four layers that were modeled) which is in direct contact with the Pd(1 1 1) surface is shown.

Rxn 6), oxidation via O*-addition to the carbon to form the ethoxide intermediate of the geminal diol (ethoxy-diol, $CH_3CH(OH)O$, Rxn 5), and further C—H activation of the C_1-carbon to form hydroxyethylidyne (CH_3COH, Rxn 7). The results from the DFT calculations indicate that all of these barriers are higher than that for the successive O—H activation to form acetaldehyde. For example, the metal-catalyzed C—H activation to form hydroxyethylidyne has a barrier of 101 kJ/mol (Rxn 7a), compared to the metal-catalyzed O—H activation to form acetaldehyde which has a barrier of 90 kJ/mol (Rxn 4a). If O* is present on the surface, it can act as a base to abstract the hydrogen of the O—H bond, forming acetaldehyde with a barrier of 107 kJ/mol (Rxn 4b). However, O* on Pd does not aid in the activation of the C—H bond which leads to hydroxyethylidyne (Rxn 7b, 148 kJ/mol), which is consistent among all C—H bond activations as was reported above. The barrier to oxidize the hydroxyethylidene intermediate via O*-addition has a barrier of 98 kJ/mol (Rxn 5). In systems operating at high pH, it is unlikely that the hydroxyethylidyne intermediate will form on the surface. If it does, however, a surface bound hydroxide species will activate the O—H bond to form acetaldehyde without an activation barrier as opposed to the route to from hydroxyethylidyne via OH*-abstraction (56 kJ/mol, Rxn 7c) or the route to form a geminal diol through OH*-addition (87 kJ/mol, Rxn 6). In summary, under the conditions studied (bare surface, with O* or OH* present), there are no paths that can proceed without passing through acetaldehyde, indicating that its presence is not the result of a side-reaction, but rather the first step in a sequential reaction.

These results suggest that different alcohol dehydrogenation paths can be operative depending upon the metal, pH, the oxygen pressure, and the temperature as they set the chemical potential and as such the surface coverage of O* and OH*. At neutral pH and low surface coverages of O*, dehydrogenation appears to proceed via metal atom insertion reactions which sequentially activate the alpha C_1—H and O—H bonds of the alcohol to form the aldehyde. However, if O* is prevalent on the surface as a result of O_2 or OOH* dissociation, the dehydrogenation initially proceeds

Table 2
Complete summary of modeled oxidation reactions.

Reaction	Pd(111)		Pd(111) aqueous[a]	
	E_{ACT}	E_{RXN}	E_{ACT}	E_{RXN}
$CH_3CH_2OH^* + * \rightarrow CH_3CH_2O^* + H^*$	106	17	131	58
$CH_3CH_2OH^* + O^* \rightarrow CH_3CH_2O^* + OH^*$	40	22	80	25
$CH_3CH_2OH^* + OH^* \rightarrow CH_3CH_2O^* + H_2O^*$	0	−25	29	−21
$CH_3CH_2OH^* + * \rightarrow CH_3CHOH^* + H^*$	50	−31	84	−3
$CH_3CH_2OH^* + O^* \rightarrow CH_3CHOH^* + OH^*$	122	−26	126	−35
$CH_3CH_2OH^* + OH^* \rightarrow CH_3CHOH^* + H_2O^*$	105	−73	64	−70
$CH_3CH_2O^* + * \rightarrow CH_3CHO^* + H^*$	53	−47	51	−65
$CH_3CH_2O^* + O^* \rightarrow CH_3CHO^* + OH^*$	73	−41	95	−97
$CH_3CH_2O^* + OH^* \rightarrow CH_3CHO^* + H_2O^*$	75	−88	60	−126
$CH_3CHOH^* + * \rightarrow CH_3CHO^* + H^*$	69	1	90	−4
$CH_3CHOH^* + O^* \rightarrow CH_3CHO^* + OH^*$	20	7	107	−36
$CH_3CHOH^* + OH^* \rightarrow CH_3CHO^* + H_2O^*$	0	−40	0	−76
$CH_3CHOH^* + O^* \rightarrow CH_3CH(OH)O^* + *$	91	−18	98	−60
$CH_3CHOH^* + OH^* \rightarrow CH_3CH(OH)_2^* + *$	74	−37	87	−63
$CH_3CHOH^* + * \rightarrow CH_3COH^* + H^*$	106	−25	101	40
$CH_3CHOH^* + O^* \rightarrow CH_3COH^* + OH^*$	121	−19	148	−12
$CH_3CHOH^* + OH^* \rightarrow CH_3COH^* + H_2O^*$	66	−66	56	−69
$CH_3CH(OH)_2^* + * \rightarrow CH_3CH(OH)O^* + H^*$	78	23	97	48
$CH_3CH(OH)_2^* + O^* \rightarrow CH_3CH(OH)O^* + OH^*$	37	29	35	2
$CH_3CH(OH)_2^* + OH^* \rightarrow CH_3CH(OH)O^* + H_2O^*$	0	−18	0	−44
$CH_3CH(OH)_2^* + * \rightarrow CH_3C(OH)_2^* + H^*$	78	−35	–	–
$CH_3CH(OH)_2^* + O^* \rightarrow CH_3C(OH)_2^* + OH^*$	00	−29	–	–
$CH_3CH(OH)_2^* + OH^* \rightarrow CH_3C(OH)_2^* + H_2O^*$	94	−76	–	–
$CH_3CHO^* + O^* \rightarrow CH_3CHOO^* + *$	41	14	83	60
$CH_3CHO^* + OH^* \rightarrow CH_3CH(OH)O^* + *$	24	−15	28	57
$CH_3CHO^* + H2O^* \rightarrow CH_3CH(OH)O^* + H^*$	80	26	–	–
$CH_3CHO^* + * \rightarrow CH_3CO^* + H^*$	22	−70	29	−30
$CH_3CHO^* + O^* \rightarrow CH_3CO^* + OH^*$	80	−65	114	−62
$CH_3CHO^* + OH^* \rightarrow CH_3CO^* + H_2O^*$	39	−111	50	−105
$CH_3CH(OH)O^* + * \rightarrow CH_3COOH^* + H^*$	11	−106	21	−146
$CH_3CH(OH)O^* + O^* \rightarrow CH_3COOH^* + OH^*$	54	−100	90	−184
$CH_3CH(OH)O^* + OH^* \rightarrow CH_3COOH^* + H_2O^*$	38	−147	86	−207
$CH_3COH^* + * \rightarrow CH_3CO^* + H^*$	62	−44	26	−54
$CH_3COH^* + O^* \rightarrow CH_3CO^* + OH^*$	24	−39	79	−86
$CH_3COH^* + OH^* \rightarrow CH_3CO^* + H_2O^*$	0	−171	17	−112
$CH_3COH^* + O^* \rightarrow CH_3COOH^* + *$	105	−90	142	−144
$CH_3COH^* + OH^* \rightarrow CH_3C(OH)_2^* + *$	72	−48	–	–
$CH_3C(OH)_2^* + * \rightarrow CH_3COOH^* + H^*$	37	−47	–	–
$CH_3C(OH)_2^* + O^* \rightarrow CH_3COOH^* + OH^*$	8	−42	–	–
$CH_3C(OH)_2^* + OH^* \rightarrow CH_3COOH^* + H_2O^*$	0	−89	–	–
$CH_3CO^* + O^* \rightarrow CH_3COO^* + *$	67	−95	74	−104
$CH_3CO^* + OH^* \rightarrow CH_3COOH^* + *$	30	−51	17	−111
$CH_3CO^* + H_2O^* \rightarrow CH_3COOH^* + H^*$	104	−9	–	–
$CH_3CHOO^* + * \rightarrow CH_3COO^* + H^*$	25	−179	7	−194
$CH_3CHOO^* + O^* \rightarrow CH_3COO^* + OH^*$	28	−174	105	−226
$CH_3CHOO^* + OH^* \rightarrow CH_3COO^* + H_2O^*$	24	−220	54	−249

Energies are reported in kJ/mol. Reactions were modeled using 21–23 solvent water molecules per unit cell to solvate the resulting intermediates, depending on the size of the reaction complex.

[a] Reactions involving dihydroxyethylidyne ($CH_3C(OH)_2$) were not modeled with solvent present as they rapidly deprotonate to form acetic acid.

via the O*-assisted activation of the O—H bond of the alcohol to form an alkoxide intermediate. At high pH, the alkoxide intermediate is formed via OH-assisted activation of the alcohol, either on the surface or in solution. In the last two cases, the C_1—H bond of the alkoxide is activated by hydride elimination onto the metal surface to form acetaldehyde.

$$\text{Low } O^*/OH^*: \quad CH_3CH_2OH^* + 2^* \rightarrow CH_3CHOH^* + H^* + * \rightarrow CH_3CH{=}O^* + 2H^* \tag{9a}$$

$$\text{High } O^*/\text{Low } OH^*: \quad CH_3CH_2OH^* + O^* + * \rightarrow CH_3CH_2O^* + OH^* + * \rightarrow CH_3CH{=}O^* + H^* + H^* \tag{9b}$$

$$\text{High } OH-: \quad CH_3CH_2OH + OH - +2^* \leftrightarrow CH_3CH_2O^* + H_2O^* + e- \rightarrow CH_3CH{=}O^* + e - + H^* + H_2O \tag{9c}$$

4.2. Acetaldehyde oxidation at high pH

The acetaldehyde that forms can desorb from the surface or react via the paths presented in Fig. 1. The desorption of acetaldehyde should occur quite readily as it is only weakly held to the surface with a binding energy of 20 kJ/mol. Once in solution, it can rapidly undergo hydration via a nucleophilic attack of OH^- on the C=O bond to form a geminal diol species ($CH_3CH(OH)_2$) [7,23] as is shown in the two-step process in Eq. (7). Fig. 3 shows the detailed changes in the structure along with the changes in energies that occur along the reaction coordinate for the conversion of acetaldehyde to ethoxy-diol in the presence of base in solution. In the reactant state, the hydroxide anion is hydrogen bonded to three nearby water molecules, whereas the carbonyl group of the aldehyde is hydrogen bonded with only two. In the product, one of the water molecules shifts to hydrogen bond to the carbonyl group of the ethoxy-diol intermediate. The cost in restructuring of water to accommodate these changes in the solvation shell along the reaction coordinate lead to an activation energy of 45 kJ/mol as previously reported [12]. The ethoxy-diol intermediate that results can subsequently protonate in solution to form the geminal diol hydrate. While the germinal diol intermediate can dehydrogenate on the surface to form acetic acid in a manner similar to that for ethanol dehydrogenation to form acetaldehyde, it has a much lower pK_a (13–14) [46] than ethanol (15.9), indicating that it would more likely to deprotonate in solution. If the germinal diol instead adsorbs on the Pd surface intact, it can subsequently be deprotonated by adsorbed OH^* to form ethoxy-diol. This reaction occurs without an activation barrier (Rxn 8c, Fig. 4). Both the solution-phase deprotonation and the OH^*-surface catalyzed deprotonation result in a strongly adsorbed ethoxy-diol intermediate on the Pd surface. This aqueous-phase hydration to form the geminal diol is thought to be equilibrated, which results in an equivalency of the two oxygens in the product acid. This helps to explain the multiple incorporations of ^{18}O isotopes into glyceric and acetic acid that occur when glycerol and ethanol oxidation is run in $H_2{}^{18}O$ [12,29]. Rather than acetaldehyde desorbing and hydrating in the aqueous phase, an alternate route via the reaction between OH^* and the aldehyde on the Pd surface to form the ethoxy-diol intermediate was examined. The barrier for the nucleophilic attack of OH^* on the adsorbed acetaldehyde was calculated to be 28 kJ/mol (Rxn 11a, Fig. 4), which is lower than the solution-phase hydration. The ethoxy-diol intermediate subsequently reacts on the Pd surface to form the acetic acid product with a barrier of only 21 kJ/mol (Rxn 12a). The mechanism involves C_1-hydride elimination onto the Pd surface and, as such, is very similar to that for the C_1-hydride elimination of the ethoxide intermediate discussed earlier (Rxn 3a).

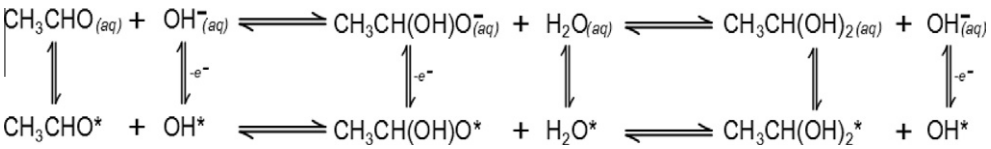

(10)

Acetaldehyde can also directly dehydrogenate to form the acetyl intermediate (CH_3CO^*, Rxn 10, Fig. 4) as is suggested in the literature [6,16,18,23]. The activation of the C—H bond to form the acetyl preferentially proceeds via a metal atom insertion reaction and results in a barrier of only 29 kJ/mol (Rxn 10a). The barriers for O^*-assisted (114 kJ/mol) and OH^*-assisted (50 kJ/mol) activation of the C—H bond are considerably higher than that over the metal as this hydrogen is not acidic. Once the acetyl is formed, it can react with OH^* on the surface to form acetic acid with a barrier of 17 kJ/mol (Rxn 15). Both oxidation pathways, through ethoxy-diol and acetyl intermediates, depend on the local OH^* coverage.

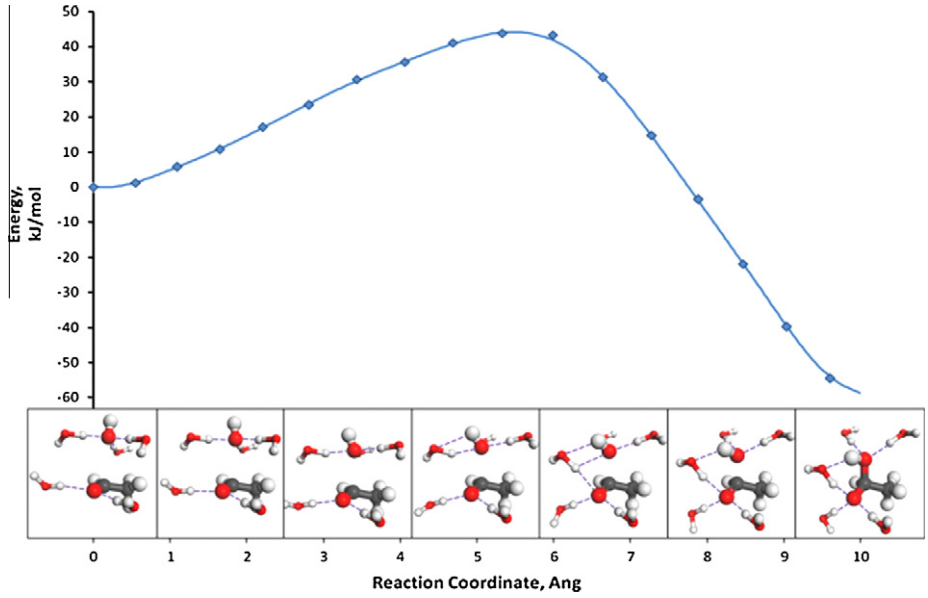

Fig. 3. Base-catalyzed oxidation of acetaldehyde in the aqueous phase. The change in energy along the reaction coordinate shows a barrier of 45 kJ/mol due to the restructuring of the water network.

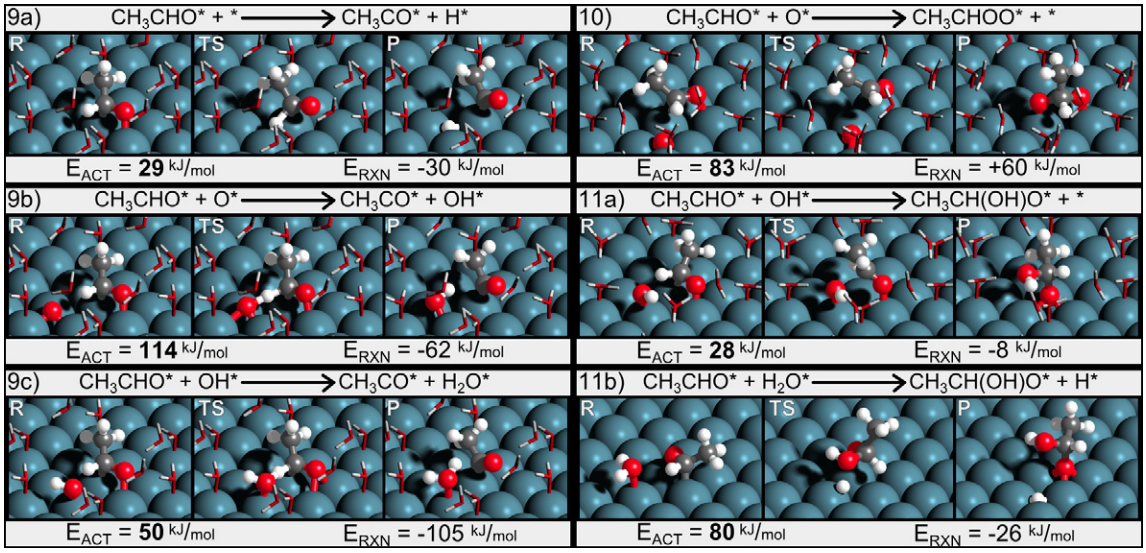

Fig. 4. Oxidation reactions of acetaldehyde over Pd(1 1 1) in the presence an aqueous media. DFT-calculated reactant, transition and product states are shown for the C—H activation, O*-addition and OH*-addition of acetaldehyde to form acetyl, dioxyethylidene and ethoxy-diol. An additional step in which acetaldehyde reacts directly with water is also shown (not modeled in solvent). While the solvent was modeled using four layers, only the layer of solvent nearest to the surface is shown in each of the figures here.

4.3. Acetaldehyde oxidation in neutral pH

If acetaldehyde desorbs, it can still react with water in solution to form the geminal diol hydrate, although the rate of reaction is slower in neutral pH. In this case, it is still believed to form the ethoxy-diol intermediate (and a proton) as shown in Eq. (11).

$$CH_3CH{=}O + 2H_2O \rightarrow CH_3CH(OH)O^- + H_3O^+ \rightarrow CH_3CH(OH)_2 + H_2O \quad (11)$$

Similarly, on the catalyst surface under neutral conditions, OH*-addition steps can still occur via the direct reaction with adsorbed water on the catalyst surface as shown in Eq. (12). However, this concerted mechanism of activating water and oxidizing the aldehyde results in a high activation barrier (80 kJ/mol) as shown in Table 2 or Fig. 3.

$$CH_3CH{=}O^* + H_2O^* \rightarrow CH_3CH(OH)O^* + H^* \quad (12a)$$

$$CH_3C{=}O^* + H_2O^* \rightarrow CH_3COOH^* + H^* \quad (12b)$$

Under these conditions, it becomes very difficult to predict whether there will be a greater concentration of O* or OH* on the surface (both of which are thought to be formed as a result of ORR), so it is also important to consider O*-addition oxidation steps along with those for OH* addition. The oxidation of acetaldehyde via the addition of O* to form dioxyethylidene (CH_3CHOO^*) has a barrier of 83 kJ/mol. This intermediate can subsequently undergo C—H activation to form the observed acetate product with a barrier of 7 kJ/mol via C_1-hydride elimination directly onto the metal surface. If the acetyl intermediate (CH_3CO^*) is formed, the O*-addition step to form acetate has a barrier of 67 kJ/mol.

4.4. Effect of O* and OH* on O—H and C—H Activations

Through the course of this study, five O—H and seven C—H activations were calculated over the model Pd(1 1 1) surface. Each of these reactions were studied on the bare metal surface, where they occur either through metal atom insertion, similar to oxidative insertion reported in organometallic catalysis [47], or through hydride elimination. The activation barriers for this mechanism (in the absence of solvent) range from 11 to 106 kJ/mol and follow a loose Brønsted–Evans–Polyani (BEP) relationship as shown in Fig. 5.

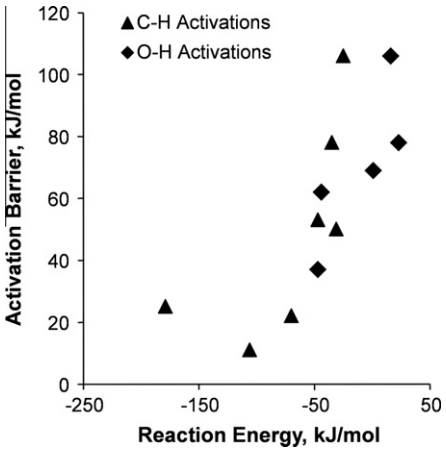

Fig. 5. Brønsted–Evans–Polyani (BEP) correlation for the activation of C—H and O—H bonds, metal-catalyzed, over the Pd(1 1 1) surface.

The C—H and O—H activations were also examined in the presence of O* and OH* which can alter the mechanism in various ways. One of these mechanisms is similar to that of σ-bond metathesis reported in organometallic systems [47]. A four-center M—C—H—O complex is formed in the transition state, indicating contributions from both metal atom insertion into the C—H bond and hydrogen atom abstraction by the O* or OH* ligand on the surface. During other activations, the metal does not act to stabilize the hydrogen; the abstraction occurs directly between the intermediate and the O* or OH*.

In all studied cases of C—H activation, the activation barrier is higher for the reactions involving the Pd—O* sites than those over Pd—Pd sites (by an average of 31 kJ/mol). Examining the transition state over the Pd—O* site pairs (examples of which are shown in Figs. 2 and 4), the O* must shift from a very stable threefold fcc site to a more active site, a near-bridge position; this comes with an energetic penalty up to 47 kJ/mol (shown in Fig. 6). The C—H bonds of alcohols are not typically acidic and as such they are not readily assisted by proton-transfer mechanisms to O* unless O* is very

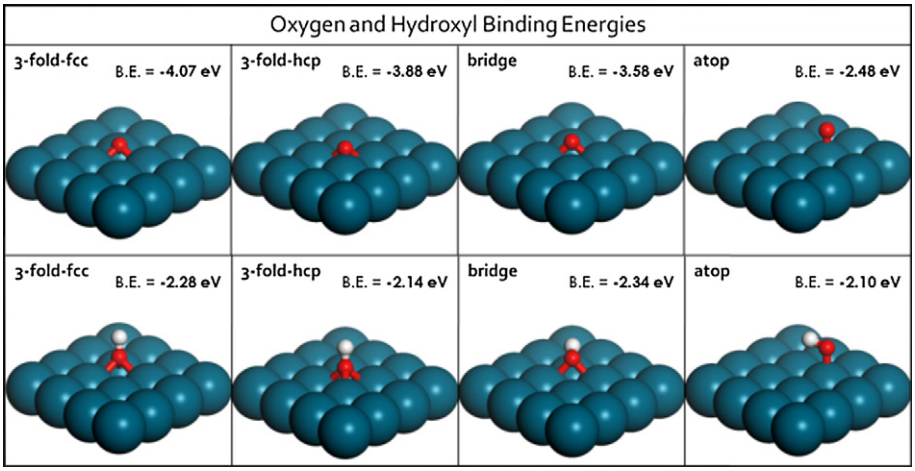

Fig. 6. Binding energy of O* and OH* at different sites on Pd(1 1 1). Atomic O* bound to the 3-fold-fcc site has the strongest binding energy and shifting it to a bridge site requires 47 kJ/mol whereas OH* is more stable on the bridge site and can shift to an atop site with only a 23 kJ/mol penalty. Four metal layers were modeled, only the top layer is shown.

basic, thus most of the activation barriers for C—H activation carried out over Pd—O* sites increase. Only on Au [12] and other coinage metals [48] do the C—H activation energies decrease via the O*-assisted mechanisms. The nearly filled d-bands for these metals lead to significant Pauli repulsive interactions in transition states and very high barriers for oxidative addition reactions. Similar repulsive interactions decrease the binding strength of O* on the coinage metals in comparison with Pd thus making it rather basic and allowing it to readily activate O—H and weakly acidic C—H bonds.

The O—H bonds, as opposed to the C—H bonds, are much more acidic, and as a result, the average barrier for O—H activation via O*-assisted proton abstraction is only 26 kJ/mol, whereas the average barrier for metal atom insertion is 70 kJ/mol, showing a significant decrease in barrier despite the energetic penalty associated with promoting the O* to an active state.

The presence of O* on Pd thus lowers the activation barriers for O—H activation but increases those for C—H activation. This difference cannot be explained through the relative strengths of the C—H and O—H bonds being studied, as the C—H bond of ethanol is 36 kJ/mol weaker than the O—H bond. The differences instead are related to the significant differences in acidity between the O—H versus C—H bonds as the abstraction reaction involves a proton transfer from the oxygenate molecule to the basic O* on the metal surface.

For OH*-assisted activation, there is no significant penalty for shifting the binding state of OH* on the Pd surface as shown in Fig. 6, in contrast to O*. The average activation barrier for the activation of C—H bonds on Pd—OH* sites is 61 kJ/mol, which is just 6 kJ/mol higher than the average on Pd—Pd sites. The small shift in activation barrier (compared to the large increase observed for O*-assisted activations) is likely due to the smaller penalty for shifting OH* to an active bridge or atop site. It is also important to note that for most cases, the metal atom insertion mechanism is the favored route for C—H activation. In contrast, all five O—H bond activations show no barrier for the reaction to take place with adsorbed OH species on Pd(1 1 1) in the absence of solvent. The basic properties of OH* and the very small penalties associated with moving OH* to an active site make it ideal for the activation of O—H bonds on a Pd surface (as well as Au and Pt [12]).

4.5. Summary of alcohol oxidation over Pd catalysts

For aqueous-phase alcohol oxidation, equilibrium is set between the ethanol and hydroxide in solution with adsorbed ethoxide as shown previously in Eq. (8). Therefore, as the pH of the system increases, the coverage of ethoxide increases on the Pd surface. This ethoxide intermediate subsequently undergoes hydride elimination on the Pd surface, resulting in the formation of acetaldehyde as well as adsorbed hydride (Eq. (10d)). Acetaldehyde subsequently hydrates in solution to form a geminal diol species. This hydration forms an ethoxy-diol intermediate, which can then adsorb on the metal surface. Acetaldehyde is formed in equilibrium with the ethoxy-diol intermediate and the geminal diol hydrate via these processes as shown in Eq. (10). The ethoxy-diol intermediate irreversibly undergoes hydride elimination on the Pd surface to form acetic acid. This mechanism, which consumes multiple hydroxide anions per turnover, is quite similar to those proposed in studies of alcohol electro-oxidation in direct alcohol fuel cells [49,50]. In systems operating at neutral or slightly acidic pH, the coverage of ethoxide on the surface is much lower, which could alter the mechanism from a base-assisted path to metal-only catalyzed route which proceeds via sequential O—H and C—H metal atom insertion steps to form hydroxyethylidene intermediate and acetaldehyde product, respectively. Following this, the rate is significantly limited by the low coverage of O* and OH* on the surface, but can proceed through the ethoxy-diol intermediate as at high pH.

4.6. Oxygen reduction reaction

As OH* appears to catalyze the O—H bond activation steps as well as the step involving oxygen-addition to the aldehyde in systems operating at high pH, oxygen (in the form of O_2 or O*) does not appear to be necessary in the direct conversion of ethanol to acetic acid over Pd, which is consistent with previous results over Au and Pt [12]. However, unlike Au, alcohol oxidation on Pd or Pt can proceed (at lower rates) at neutral or slightly acidic pH [23,24]. Furthermore, alcohol oxidation, when carried out over Pd at low pH, generates hydride intermediates on the surface, which may not form when the reaction takes place over Au. The alcohol oxidation sequence also transfers four electrons into the Pd catalyst, which must be removed (along with the hydrogen intermediates) in order to close the catalytic cycle and preserve activity. This occurs via the reduction of molecular oxygen. In general, the reduction reaction must dissociate O_2 and add hydrogen atoms to the intermediates to form one of three products: water, the most studied and common product of ORR due to its application in fuel cells; hydroxide, replenishing the supply consumed as a result of the alcohol the oxidation; or hydrogen peroxide, an observed by-prod-

Table 3
Complete summary of modeled ORR reactions.

Reaction	Pd(111)		Pd(111) aqueous[a]	
	E_{ACT}	E_{RXN}	E_{ACT}	E_{RXN}
$O_2^* + * \rightarrow 2O^*$	65	−161	54	−171
$O_2^* + H^* \rightarrow OOH^* + H^*$	85	15	110	−29
$O_2^* + H_2O^* \rightarrow OOH^* + OH^*$	25	24	37	35
$OOH^* + * \rightarrow O^* + OH^*$	4	−171	44	−176
$OOH^* + H^* \rightarrow H_2O_2^* + *$	70	3	76	−9
$OOH^* + H_2O^* \rightarrow H_2O_2^* + OH^*$	48	44	44	0
$H_2O_2^* + * \rightarrow 2OH^*$	4	−168	5	−199
$O^* + H^* \rightarrow OH^*$	104	5	99	−32
$O^* + H_2O^* \rightarrow 2OH^*$	50	47	69	39
$OH^* + H^* \rightarrow H_2O^* + *$	66	−41	77	71

Energies are reported in kJ/mol.
[a] Reactions with H_2O^* in the reactants were modeled with 22 water molecules, otherwise 23 water molecule were modeled as the solvent.

uct in fuel cells and alcohol oxidation over Au [11,12]. Each of these three products can remove electrons and adsorbed hydrogen from the catalyst, so it is important to consider the entire reaction network. Table 3 shows all of the elementary steps that were studied along with their reaction energies and activation barriers in the presence and absence of solvent on the Pd(111) surface.

Molecular oxygen binds to Pd with an energy of 75 kJ/mol and can readily dissociate to form two oxygen adatoms with a barrier of 54 kJ/mol with solvent present and 65 kJ/mol without solvent (Rxn O1), which is similar to that reported previously [25,51]. While the O^* can subsequently react with H^* to form OH^*, the barrier is rather high at 110 kJ/mol. Alternatively, O^* can be reduced through the direct reaction with the water solvent: $O^* + H_2O^* \rightarrow 2OH^*$ (Rxn O6b), which has a barrier of 69 kJ/mol. Instead of initial dissociation, O_2 can undergo an initial reduction to form a peroxide (OOH^*) intermediate. This reduction can occur via the reaction with H^* (E_{ACT} = 110 kJ/mol, Rxn O3a) or through the reaction with H_2O (37 kJ/mol, Rxn O3b). Once formed, OOH^* easily dissociates in a strongly exothermic reaction to form O^* and OH^* with a barrier of 20 kJ/mol. The resulting O^* can (as before) be reduced through reaction with water from the solvent. These two processes leading to hydroxide, shown in Eq. (11), are both limited by the O—O cleavage step, with overall energy barriers of 54 and 55 kJ/mol, respectively. Once OH^* is formed, it can react with H^* on the surface to form water, with a barrier of 77 kJ/mol, consuming H^* which is produced in the oxidation reactions. However, as only 2–3 H^* are produced via the oxidation process discussed above, not all of the OH^* will be fully reduced to H_2O thus regenerating some OH^* consumed during oxidation.

$$O_2^* + 2H_2O^* \rightarrow 2O^* + 2H_2O^* \rightarrow 4OH^* \quad (11a)$$

$$O_2^* + 2H_2O^* \rightarrow OH^* + OOH^* + H_2O^* \rightarrow 2OH^* + O^* + H_2O^* \rightarrow 4OH^* \quad (11b)$$

$$OH^* + H^* \rightarrow H_2O^* \quad (11c)$$

The formation of H_2O_2 was found to be unlikely over Pd at these conditions, as the further reduction barriers (shown in Table 3) are rather high compared to the dissociation barrier, this is in contrast to the recent work on Au [12], but is consistent with experimental studies which showed very little rates of peroxide production during glycerol oxidation on Pd [52].

4.7. Coverage effects

While these calculations take into account the effect of solvent, they are run at the relatively low coverage of 1/9 ML. Under working conditions, the surface may be partially covered by different intermediates, likely hydroxide, ethoxide or atomic oxygen. The effect of these intermediates was not explicitly modeled here. High surface coverages of any of these intermediates will act to block Pd metal sites and inhibit reactions that take place over Pd—Pd sites, such as O_2 dissociation, oxidative insertion reactions and hydride elimination. Increased coverages of oxygen or hydroxide will improve the likelihood O—H activations from proton-transfer reactions (such as Rxn 1b, 1c). Furthermore, as the coverage of oxygen increases, so does its basicity, due to adsorbate–adsorbate repulsion. While the binding energy of hydroxide or ethoxide is strong (−2.73 and −1.45 eV, respectively), this binding energy is referenced to a gas-phase hydroxide or ethoxide rather than the solution-phase species. Due to this approximation, the changes in the solvation energy upon adsorption are not accounted for and strong ΔG_{solv} for those anions have been reported in literature [53]. However, solvation energies of the surface bound species are also likely to be strong, as they can still form up to three hydrogen bonds with surrounding water molecules, in order to account for this solvation energy of an adsorbed species, dynamic calculations would have to be performed to statistically sample a large ensemble of possible solvent structures which is outside of the scope of this work.

Additionally, these calculations do not take into account entropic effects on these reaction paths. It is expected that entropy will reduce the free energy of adsorption for species which are stable in solution such as ethanol, ethoxide, and hydroxide. Furthermore, reaction and activation energies involving weakly bound intermediates may be slightly under-predicted due to the increased entropy in the reactant state. However, the entropic changes that occur should not alter the conclusions of this work.

5. Conclusions

Alcohol oxidation on Pd is catalytically promoted by the presence of base as hydroxide catalyzes deprotonation and increasing the pH increases the coverage of alkoxy intermediates on the surface through equilibrium. The alkoxy intermediate undergoes an irreversible hydride transfer on the catalyst surface to form an aldehyde. The oxidation reaction proceeds via a base-catalyzed nucleophilic addition to the aldehyde to form an alkoxy intermediate from the geminal diol in solution or on the surface. The equilibrium between the resulting alkoxy-diol intermediate and geminal diol species offers an explanation for the multiple incorporations of ^{18}O in the product acid that is found experimentally. Finally, the alkoxy-diol intermediate irreversibly dehydrogenates to form a carboxylic acid on the catalyst surface. This carboxylic acid is in equilibrium with the experimentally-observed carboxylate-cation adduct. This mechanism is consistent with the mechanism reported previously for Au-catalyzed alcohol oxidation [12].

In systems operating at neutral or slightly acidic pH, hydroxide (in solution or on the surface) is present in very low concentration, forcing the mechanism to take a different route. The dehydrogenation initially proceeds via metal atom insertion into the C—H bond with a barrier of 84 kJ/mol, forming the hydroxyethylidene intermediate which subsequently undergoes O—H activation by the metal to form acetaldehyde. Acetaldehyde further dehydrogenates to form an acetyl intermediate which subsequently reacts with a surface O^* to form acetate with a barrier of 74 kJ/mol. Alternatively, if the O^* intermediate is first reduced to form OH^*, the acetyl intermediate can react with OH^* to form acetic acid with an overall

barrier of 69 kJ/mol, which is very similar to the barrier to form acetate. In either case, the barriers for this process are higher than those with hydroxide present, consistent with experimental findings which demonstrate first-order kinetics with the concentration of hydroxide.

The role of O_2 in this system is to remove the electrons that form on the surface as a result of the oxidation of the alcohol through the reduction of oxygen by water. This regenerates hydroxide intermediates and removes the H^* produced during oxidation. The presence of an aqueous environment diminishes the dissociative-reduction of oxygen but favors the associative-reduction. The combination of the alkaline environment along with the Pd surface provides unique opportunities for mechanisms which involve direct interaction with the solvent or hydroxide species present in aqueous media, such as the reduction of O_2^* with H_2O to form $^*OOH$ intermediates.

The alcohol oxidation and O_2 reduction mechanisms reported here for the catalytic oxidation of alcohols in basic media are quite similar to those involved in the electrocatalytic oxidation and reduction reactions that occur in alkaline fuel cells. In these aqueous-phase reactions at high pH, the combination of the solvent and ionic species creates a potential on the catalyst surface which is often neglected in heterogeneous catalysis.

Acknowledgments

We are grateful to the National Science Foundation for the financial support of this work through the NSF PIRE program (OISE-0730277) and NSF Center for Biorenewable Chemicals (EEC-0813570) and to the Environmental Molecular Science Laboratory, a national scientific user facility sponsored by the DOE's Office of Biological and Environmental Research located at Pacific Northwest National Laboratory for supercomputing time. We would also like to thank Professor Robert J. Davis, Dr. Bhushan Zope and Ms. Sara Davis for helpful discussions.

References

[1] A.J. Ragauskas, C.K. Williams, B.H. Davison, G. Britovsek, J. Cairney, C.a. Eckert, W.J. Frederick, J.P. Hallett, D.J. Leak, C.L. Liotta, J.R. Mielenz, R. Murphy, R. Templer, T. Tschaplinski, Science 311 (2006) 484–489.
[2] G.W. Huber, S. Iborra, A. Corma, Chem. Rev. 106 (2006) 4044–4098.
[3] Y. Zheng, X. Chen, Y. Shen, Chem. Rev. 108 (2008) 5253–5277.
[4] Y. Román-Leshkov, J.N. Chheda, J.a. Dumesic, Science 312 (2006) 1933–1937.
[5] S.E. Davis, L.R. Houk, E.C. Tamargo, A.K. Datye, R.J. Davis, Catal. Today 160 (2011) 55–60.
[6] T. Mallat, A. Baiker, Chem. Rev. 104 (2004) 3037–3058.
[7] M. Besson, P. Gallezot, Catal. Today 57 (2000) 127–141.
[8] J.-D. Grunwaldt, M. Caravati, A. Baiker, J. Phys. Chem. B 110 (2006) 25586–25589.
[9] P. Haider, J.-D. Grunwaldt, R. Seidel, A. Baiker, J. Catal. 250 (2007) 313–323.
[10] A. Corma, H. Garcia, Chem. Soc. Rev. 37 (2008) 2096–2126.
[11] W.C. Ketchie, M. Murayama, R.J. Davis, Top. Catal. 44 (2007) 307–317.
[12] B.N. Zope, D.D. Hibbitts, M. Neurock, R.J. Davis, Science 330 (2010) 74–78.
[13] S. Demirel-Gulen, M. Lucas, P. Claus, Catal. Today 102 (2005) 166–172.
[14] S. Carrettin, P. McMorn, P. Johnston, K. Griffin, G.J. Hutchings, Chem. Commun. (2002) 696–697.
[15] C. Alonso, J. Gonzalez-Velsasco, Z. Phys. Chemie 4 (1990) 799–822.
[16] C. Bianchini, P.K. Shen, Chem. Rev. 109 (2009) 4183–4206.
[17] G. Cui, S. Song, P.K. Shen, A. Kowal, C. Bianchini, J. Phys. Chem. C 113 (2009) 15639–15642.
[18] Z.X. Liang, T.S. Zhao, J.B. Xu, L.D. Zhu, Electrochim. Acta 54 (2009) 2203–2208.
[19] J.H.J. Kluytmans, A.P. Markusse, B.F.M. Kuster, G.B. Marin, J.C. Schouten, Catal. Today 57 (2000) 143–155.
[20] E. Yeager, Electrochim. Acta 29 (1984) 1527–1537.
[21] R.R. Adžić, J.X. Wang, J. Phys. Chem. B 102 (1998) 8988–8993.
[22] X. Deng, B.K. Min, A. Guloy, C.M. Friend, J. Am. Chem. Soc. 127 (2005) 9267–9270.
[23] V.R. Gangwal, J. van der Schaaf, B.F.M. Kuster, J.C. Schouten, J. Catal. 229 (2005) 389–403.
[24] R. Garcia, M. Besson, P. Gallezot, Appl. Catal. A 127 (1995) 165–176.
[25] W. Tang, G. Henkelman, J. Chem. Phys. 130 (2009) 194504.
[26] F.C. Simões, D.M. dos Anjos, F. Vigier, J.-M. Léger, F. Hahn, C. Coutanceau, E.R. Gonzalez, G. Tremiliosi-Filho, A.R. de Andrade, P. Olivi, K.B. Kokoh, J. Power Sources 167 (2007) 1–10.
[27] P.J.M. Dijkgraaf, H.A.M. Duisters, B.F.M. Kuster, K. van der Wiele, J. Catal. 112 (1988) 337–344.
[28] A. Markusse, B. Kuster, J. Schouten, Stud. Surf. Sci. Catal. 126 (1999) 273–280.
[29] M. Rottenburg, P. Baertschi, Helv. Chim. Acta 39 (1956) 1973–1975.
[30] P. Vinke, D. de Wit, A.T.J.W. de Goede, H. van Bekkum, Stud. Surf. Sci. Catal. 72 (1992) 1–20.
[31] R. DiCosimo, G.M. Whitesides, J. Phys. Chem. 93 (1989) 768–775.
[32] H.E. van Dam, L.J. Wisse, H. van Bekkum, Appl. Catal. 61 (1990) 187–197.
[33] M. Hayashi, K. Yamada, S. Nakayama, H. Hayashi, S. Yamazaki, Grn. Chem. 2 (2000) 257–260.
[34] C. Keresszegi, T. Burgi, T. Mallat, A. Baiker, J. Catal. 211 (2002) 244–251.
[35] G. Kresse, J. Furthmuller, Comp. Mater. Sci. 6 (1996) 15–50.
[36] M. Methfessel, A. Paxton, Phys. Rev. B: Condens. Matter Mater. Phys. 40 (1989) 3616–3621.
[37] P.E. Blochl, O. Jepsen, O.K. Andersen, Phys. Rev. B: Condens. Matter Mater. Phys. 49 (1994) 16223–16233.
[38] D. Vanderbilt, Phys. Rev. B: Condens. Matter Mater. Phys. 41 (1990) 7892–7895.
[39] G. Kresse, J. Hafner, J. Phys.: Condens. Matter 6 (1994) 8245–8257.
[40] J.P. Perdew, J.A. Chevary, S.H. Vosko, K.A. Jackson, M.R. Pederson, D.J. Singh, C. Fiolhais, Phys. Rev. B: Condens. Matter Mater. Phys. 46 (1992) 6671–6686.
[41] P. Vassilev, R.a. van Santen, M.T.M. Koper, J. Chem. Phys. 122 (2005) 54701.
[42] J.-S. Filhol, M. Neurock, Angew. Chem., Int. Ed. 118 (2006) 416–420.
[43] C.D. Taylor, M.J. Janik, M. Neurock, R.G. Kelly, Mol. Simul. 33 (2007) 429–436.
[44] H. Jonsson, G. Mills, H. Jónsson, K.W. Jacobsen, Classical and quantum dynamics in condensed phase simulations, in: Proceedings of the International School of Physics, 1998, pp. 385–404.
[45] G. Henkelman, H. Jónsson, J. Chem. Phys. 111 (1999) 7010.
[46] G. Kortum, W. Vogel, K. Andussow, Dissociation Constants of Organic Acids in Aqueous Solution, Butterworth, New York, NY, 1961.
[47] T.R. Cundari, T.V. Grimes, T.B. Gunnoe, J. Am. Chem. Soc. 129 (2007) 13172–13182.
[48] J.T. Roberts, R.J. Madix, in: R.J. Madix (Ed.), Surface Reactions, Springer-Verlag, New York, NY, 1994.
[49] C. Coutanceau, L. Demarconnay, C. Lamy, J.-M. Léger, J. Power Sources 156 (2006) 14–19.
[50] V. Bambagioni, C. Bianchini, J. Filippi, W. Oberhauser, A. Marchionni, F. Vizza, R. Psaro, L. Sordelli, M.L. Foresti, M. Innocenti, ChemSusChem 2 (2009) 99–112.
[51] H.C. Ham, G.S. Hwang, J. Han, S.W. Nam, T.H. Lim, J. Phys. Chem. C 113 (2009) 12943–12945.
[52] W.C. Ketchie, M. Murayama, R.J. Davis, J. Catal. 250 (2007) 264–273.
[53] J.R. Pliego, M. Riveros, Chem. Phys. Lett. 332 (2000) 597–602.